

Second-order topological non-Hermitian skin effects

Ryo Okugawa,¹ Ryo Takahashi,² and Kazuki Yokomizo²

¹Graduate School of Information Sciences, Tohoku University, Sendai 980-8579, Japan

²Department of Physics, Tokyo Institute of Technology,
2-12-1 Ookayama, Meguro-ku, Tokyo, 152-8551, Japan

(Dated: August 11, 2020)

Higher-order topology realizes topologically robust corner modes as manifestation of the nontriviality. We theoretically propose non-Hermitian skin effects which stem from second-order topology of chiral-symmetric Hermitian systems. It is found that the skin modes are localized at corners. We demonstrate two types of the second-order topological skin effects by two-dimensional intrinsic and extrinsic second-order topology. The intrinsic second-order topological skin effect is characterized topologically by bulk inversion symmetry as well as chiral symmetry. Meanwhile, the extrinsic second-order topological skin effect occurs from topological correspondence between edges and corners. We show that the non-Hermitian skin modes emerge by using a relationship between the second-order and the conventional first-order topology.

Introduction. Since discovery of the quantum spin Hall insulator [1–4], many topological phases have been studied theoretically and experimentally [5–8]. The concept of topological phases has been recently generalized to higher-order topology and non-Hermitian topology. In n th-order topological phases in d -dimensional systems, topologically protected states appear at the $(d - n)$ -dimensional boundaries such as corners [9–36]. Meanwhile, non-Hermiticity enriches topological phenomena which do not emerge in Hermitian systems [37, 38]. Such examples are exceptional points [39–65] and skin effects [32, 33, 36, 66–91].

Higher-order topological phases are classified into two types: *intrinsic* and *extrinsic*. Intrinsic higher-order topology can be determined by the bulk band structures. Namely, the intrinsic higher-order topological boundary modes are stable as long as the bulk gap is open [12–18, 21, 22, 31]. If symmetry protecting the higher-order topology is preserved, the topological characterization is independent of crystal termination. By contrast, extrinsic higher-order topology depends on crystal termination. Thus, when the surfaces and edges close the band gap, extrinsic higher-order topology can change unlike intrinsic one [9, 10, 19, 21–25]. Accordingly, extrinsic higher-order topological corner modes generally stem from nontriviality in the edges [13, 21–24].

In non-Hermitian systems, the complex spectra provide new topological classification based on point gap [63, 66, 77, 78, 92–94]. Point-gap topology indicates how a non-Hermitian Hamiltonian can be deformed to a unitary matrix. Therefore, topological phenomena characterized by a point gap is unique to non-Hermitian systems. Interestingly, non-Hermitian skin effect is one of the point-gap topological examples [66, 71, 77, 78, 81–83].

The skin effect is a remarkable difference between energy spectra under a periodic boundary condition (PBC) and those under an open boundary condition (OBC). For a large open system, we can analyze the non-Hermitian energy spectrum by complex wavevectors k

[67, 72]. In one-dimensional (1D) systems, the value of $\beta \equiv e^{ik}$ is confined on a loop on the complex plane. The loop is named generalized Brillouin zone. Because non-Hermitian eigenstates can have the complex wavevectors, the eigenstates called skin modes are localized at either end of the system under the OBC [67]. Importantly, non-Hermitian skin effect leads to many intriguing phenomena including nonreciprocal transport [73, 88–91].

There are two approaches to detect non-Hermitian skin effects. As mentioned above, one is to directly compute the generalized Brillouin zone to describe the localization [32, 67, 68, 72, 74, 79, 81, 82]. However, it is difficult, especially in high-dimensional systems with many bands. Another is to employ a topological invariant for point-gap topology [66, 71, 77, 81–83]. A nontrivial invariant for a point gap typically tells that skin effect occurs. Because point-gap topology gives a simple understanding of skin effects, the approach can be extended to various systems. Hence, we take the topological approach to generally explore skin effects.

In this paper, we suggest skin effects characterized by second-order topology. Our study connects non-Hermitian point-gap topology and Hermitian higher-order topology. We study skin modes localized at corners by using intrinsic and extrinsic second-order topology. The work opens a new route to discover non-Hermitian topological skin effects with higher-order topology.

Topology of skin effects. Because skin effects originate from point-gap topology, we introduce the non-Hermitian topological characterization by the point gap [66, 77, 94]. A point gap for a Hamiltonian H is open if $\det(H - E) \neq 0$ at a reference energy E . Point-gap topology for a non-Hermitian Hamiltonian H at E is given from the following extended Hermitian Hamiltonian defined as

$$\tilde{H} = \begin{pmatrix} 0 & H - E \\ H^\dagger - E^* & 0 \end{pmatrix}. \quad (1)$$

The point-gap topology for H coincides with Hermitian topology for the extended Hermitian Hamiltonian \tilde{H} .

The extended Hermitian Hamiltonian has diagonal chiral symmetry represented as $\Gamma = \text{diag}(1, -1)$. Therefore, 1D non-Hermitian systems without any symmetries can be classified by the winding number for the 1D Hermitian systems with chiral symmetry. The integer winding number for the PBC is [66, 77, 81, 82, 94]

$$W(E) = \int_0^{2\pi} \frac{dk}{2\pi i} \frac{d}{dk} \log \det(H(k) - E). \quad (2)$$

If there is a reference energy with the nonzero $W(E)$, skin effect occurs as manifestation of the nontrivial topology [77, 81].

We extend this idea to second-order topology with the winding number. In some higher-order topological phases, the topology is understandable as generalization of that for 1D chiral-symmetric systems. When we have a chiral-symmetric Hermitian Hamiltonian \tilde{H} which realizes the second-order topological phase, we can extract the corresponding nontrivial non-Hermitian Hamiltonian H . Then, H shows skin modes for the second-order topology.

Intrinsic second-order topological skin effect. First, we investigate skin effect with intrinsic second-order topology characterized by inversion symmetry. When a two-dimensional (2D) chiral-symmetric Hermitian system has inversion symmetry, intrinsic second-order topology is allowed if the operators of the two symmetries anti-commute [16, 18]. The topological zero-energy corner modes are protected by the bulk topology. By using the second-order topology for point gap, we show that non-Hermitian systems can have skin modes localized at the corner.

Before going to a detail of the skin effect, we explain bulk-corner correspondence of the intrinsic second-order topology in Hermitian systems. We assume that Hermitian Hamiltonian \tilde{H} has inversion symmetry \tilde{I} which gives $\tilde{I}\tilde{H}(\mathbf{k})\tilde{I}^\dagger = \tilde{H}(-\mathbf{k})$ in addition to chiral symmetry Γ . Such systems are characterized by double band inversion, which means that band touchings invert two conduction and two valence bands with the opposite parity eigenvalues [15–18, 27–29, 31, 95]. The double band inversion induces topological bulk structures with the intrinsic second-order topology for corner modes. To relate the double band inversion to the winding number in Eq. (2), we introduce the following bulk topological invariants defined as [96]

$$\mu_{j=x,y} = n_-(0, 0) - n_-(\pi, \pi) + s_j \{n_-(\pi, 0) - n_-(0, \pi)\} \quad (3)$$

where $n_-(\Gamma_i)$ is the number of states with odd parity below zero energy at the inversion invariant momentum Γ_i , and $s_{x(y)} = +1(-1)$. The parity invariant $\mu_{x(y)}$ can detect the winding number for the ribbon geometry open in the $x(y)$ direction if the ribbon retains inversion symmetry. Significantly, $\mu_j/2$ is equal to the winding number

for 1D ribbon geometry modulo 2 when the bulk is not first-order topological. For instance, the winding number is always nonzero if $\mu_j = 2$. Hence, the 1D ribbon geometry hosts zero modes, i.e. the topological corner states, thanks to the nonzero winding number.

From the above discussion, when a non-Hermitian Hamiltonian H gives the extended Hermitian Hamiltonian \tilde{H} with the nontrivial parity invariant, H has the nonzero winding number under the OBC. Thus, the non-Hermitian system exhibits skin modes localized at the corner. Hereafter, we demonstrate the skin effect with the intrinsic second-order topology. We study the following 2D Hamiltonian under the PBC:

$$H_{int}(\mathbf{k}) = (m - c \sum_{j=x,y} \cos k_j) \sigma_0 + it \sin k_y \sigma_x + it \sin k_x \sigma_y - B_x \sigma_x - B_y \sigma_y, \quad (4)$$

where t, c, m and $\mathbf{B} = (B_x, B_y)$ are real parameters. For simplicity, we set all the parameters positive. Here, $\sigma_{x,y,z}$ are Pauli matrices, and σ_0 is the identity matrix. The extended Hermitian Hamiltonian is

$$\begin{aligned} \tilde{H}_{int}(\mathbf{k}) = & (m - \text{Re}E - c \sum_{j=x,y} \cos k_j) \sigma_x \otimes \sigma_0 \\ & - t \sin k_y \sigma_y \otimes \sigma_x - t \sin k_x \sigma_y \otimes \sigma_y \\ & - B_x \sigma_x \otimes \sigma_x - B_y \sigma_x \otimes \sigma_y + (\text{Im}E) \sigma_y \otimes \sigma_0. \end{aligned} \quad (5)$$

Only when the reference energy E is real, the Hermitian Hamiltonian has inversion symmetry represented by $\tilde{I} = \sigma_x \otimes \sigma_0$. Because $n_-(0, \pi) = n_-(\pi, 0)$ in this model, we put $\mu = \mu_x = \mu_y$. Thus, we can search for E for the nonzero winding number with the invariant μ , independently of which direction is open. Although E can deviate from the real axis, the winding number does not change unless the point gap closes.

We assume that $|\mathbf{B}|$ is sufficiently smaller than the other parameters. Then, the model under the PBC can have $\mu(E) = 2$ and trivial first-order topology for the real E when E is in the region $(m - 2c - |\mathbf{B}|, m - |\mathbf{B}|)$ or $(m + |\mathbf{B}|, m + 2c - |\mathbf{B}|)$. The detail is in the Supplemental Material [96]. Thus, the model has nonzero winding number in the inversion-symmetric ribbon geometry with one direction open. We put $m = t = c = 1$ and $B_x = B_y = 0.1$ to calculate second-order topological skin modes. Figure 1 shows the energy spectrum under various boundary conditions. In contrast to the spectrum under the PBC and the ribbon geometry in Figs. 1 (a) and (b), skin modes are widely distributed under the full OBC in Fig. 1 (c). We can see that the skin effect occurs around the energy region with $\mu = 2$. As seen in Fig. 1(d), the skin modes are localized at the corner. The skin modes are localized at one corner in each of the regions with the intrinsic second-order topology.

Here, we discuss the inversion symmetry in the extended Hermitian Hamiltonian. The original

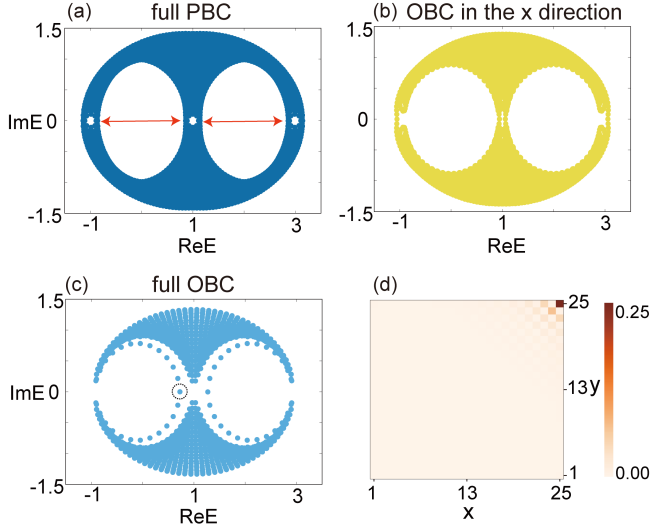


FIG. 1. (a), (b) and (c) Energy spectra of the non-Hermitian Hamiltonian H_{int} under the PBC, the OBC only in the x direction, and the full OBC. The arrows in (a) indicate the regions with $\mu = 2$ where the first-order topology is trivial. In (c), we can find the second-order topological skin modes. (d) Amplitude of the skin mode in the dotted circle in (c). The axes x and y represent the coordinates.

non-Hermitian Hamiltonian $H_{int}(\mathbf{k})$ in Eq. (4) is not inversion-symmetric. However, $H_{int}(\mathbf{k})$ satisfies $H_{int}(\mathbf{k}) = U_I H_{int}^\dagger(-\mathbf{k}) U_I^\dagger$ with the unitary matrix $U_I = \sigma_0$ with $U_I^2 = 1$. Then, the extended Hermitian Hamiltonian with a real reference energy obtains inversion symmetry represented by

$$\tilde{I} = \begin{pmatrix} 0 & U_I \\ U_I & 0 \end{pmatrix}, \quad (6)$$

where $\tilde{I}^2 = \tilde{I}\tilde{I}^\dagger = 1$ and $\Gamma\tilde{I}\Gamma^{-1} = -\tilde{I}$. The above conditions generally give the inversion operator anticommute with the chiral operator in extended Hermitian Hamiltonians.

Extrinsic second-order topological skin effect. Next, we study skin effect whose origin is extrinsic second-order topology characterized only by chiral symmetry. In the extrinsic higher-order topological phase, the edges are topologically nontrivial while the bulk is trivial [13, 21–25]. In other words, the edge bands are topological in view of the 1D first-order topology from chiral symmetry. The edge-corner correspondence produces topological corner modes through edge gap-closing at zero energy. Thus, the nontrivial topology on the 1D edges can be used for skin modes localized at the corners.

To see skin effect with the extrinsic higher-order topology, we use a 2D second-order topological Hermitian Hamiltonian whose topological edge gap-closing is analytically obtainable [23–25]. The Hamiltonian is

$$\tilde{H}'_{ext}(\mathbf{k}) = \mathcal{H}_x(k_x) \otimes 1_y + \Pi_x \otimes \mathcal{H}_y(k_y), \quad (7)$$

where $\mathcal{H}_x(k_x)$ and $\mathcal{H}_y(k_y)$ are Hermitian matrices with chiral symmetry which we write as Π_x and Π_y , respectively. 1_y is the identity matrix with the same size as \mathcal{H}_y . Then, $\tilde{H}'_{ext}(\mathbf{k})$ has chiral symmetry $\Pi = \Pi_x \otimes \Pi_y$. When we impose a semi-infinite OBC with a right-angled corner, the number of corner states are characterized by a \mathbb{Z} topological invariant [23–25]

$$\nu_{2D} = w_x w_y, \quad (8)$$

where $w_{i=x,y}$ are conventional winding numbers for the chiral-symmetric Hermitian matrices $\mathcal{H}_i(k_i)$. The topological invariant ν_{2D} changes when the edges close the gap at zero energy as well as the bulk [23–25]. Therefore, the edge gap-closing gives nonzero winding numbers for the edge bands whose topology corresponds to the extrinsic second-order topology [96].

When a non-Hermitian Hamiltonian gives the extended Hermitian Hamiltonian with the extrinsic second-order topology, the edge nontriviality gives rise to skin modes localized at the corner. To confirm our theory, we study the following 2D non-Hermitian Hamiltonian:

$$H_{ext}(\mathbf{k}) = 2t_x \cos k_x \tau_0 - 2ig_y \sin k_y \tau_x - 2it_y \cos k_y \tau_y - 2ig_x \sin k_x \tau_z, \quad (9)$$

where $t_{x,y}$ and $g_{x,y}$ are real parameters. We assume that t_x and t_y are positive for simplicity. $\tau_{x,y,z}$ are Pauli matrices, and τ_0 is the identity matrix. The extended Hermitian Hamiltonian with H_{ext} can show the second-order topology given by ν_{2D} in Eq. (8).

We impose OBCs with parallel edges on the model to see the nontrivial topology. We study the real E since the winding number is unchanged if the point gap keeps open. In this model, $(w_x(E), w_y(E)) = (-\text{sgn}(g_x), -\text{sgn}(g_y))$ when $|E| < 2t_x$, and otherwise $(w_x(E), w_y(E)) = (0, -\text{sgn}(g_y))$. Therefore, the energy real axis in $|E| < 2t_x$ has the extrinsic second-order topology with $\nu_{2D}(E) = \text{sgn}(g_x g_y)$ because of the nontrivial edges. When the topology changes on the real axis, the point gap closes at $E = \pm 2t_x$ on the edges open in the y direction but periodic in the x direction. We analyze the second-order topology by studying change of ν_{2D} in the Supplemental Material [96].

We compute energy spectra of the non-Hermitian Hamiltonian H_{ext} under different boundary conditions. We set the parameters $(t_x, g_x, t_y, g_y) = (1.0, 0.9, 0.8, 0.7)$ for the calculation. The model in Eq. (9) is topologically trivial under the full PBC, as shown in Fig. 2 (a). Thus, skin effect does not happen when we impose the OBC either in the x or in the y direction [Figs. 2 (b) and (c)]. However, Fig. 2 (c) shows that under the OBC in the y direction, the edge spectra give the nonzero winding numbers. We emphasize that the winding structures consist of the two edges parallel to the x direction. In Fig. 2(d), we can see skin modes under the full OBC near

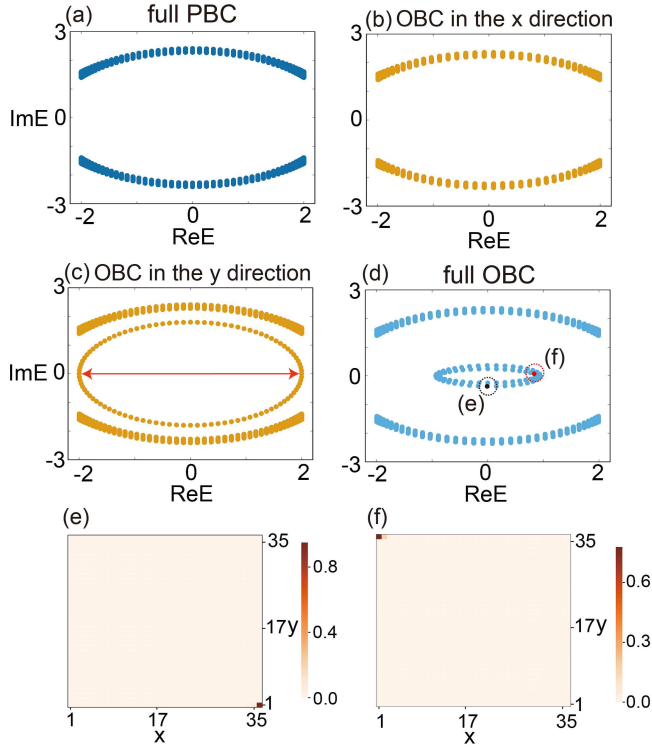


FIG. 2. Energy spectra of the non-Hermitian Hamiltonian H_{ext} under (a) the full PBC, (b) the OBC only in the x direction, (c) the OBC only in the y direction, and (d) the full OBC. When the y direction is open, each of the periodic edges has the nonzero winding number due to the nonzero ν_{2D} indicated by the arrow in (c). The skin modes can be found under the full OBC. (e) and (f) Amplitude of the black and the red skin modes in the dotted circles in (d). Each of the skin modes are localized at the opposite corners because the two edge spectra contribute to the skin effect.

the region with the nonzero $\nu_{2D}(E)$. Because the system has the two nontrivial edges in this model, each of the edges contribute to the skin effect. Hence, we can find two kinds of the skin modes which are localized at the different corners [Figs. 2 (e) and (f)], unlike the intrinsic second-order topological skin modes.

Conclusion and Discussion. In the present paper, we have proposed non-Hermitian skin modes localized at the corner by second-order topology of chiral-symmetric Hermitian Hamiltonians. We have elucidated intrinsic and extrinsic second-order topological skin effects. The intrinsic second-order topological skin effects can be detected by inversion symmetry. The extrinsic second-order topological skin effects can be understood from edge-corner correspondence. By using our theory, we can generally construct non-Hermitian Hamiltonians for the second-order topological skin effects.

Some works also discussed skin modes localized at corners under the full open boundary condition [33, 71]. The skin effect in the previous works occurs even if one direction is periodic because they are understood as skin

modes of first-order topological skin modes. In comparison with the previous works, we have predicted skin effects characterized only by the second-order topology. Moreover, since our theory defines the second-order topological invariants for each reference energy, they allow us to easily find the skin modes under full open boundary conditions.

For both the intrinsic and the extrinsic cases, we can understand the nontrivial skin effects by connecting the second-order topology to the conventional topology for the one-dimensional chiral-symmetric systems. However, the topological structures are different. The intrinsic second-order topology stems from nontrivial energy spectrum under the full periodic boundary condition. As a result, the ribbon geometry open in one direction has the nonzero winding number which leads to the skin modes. Meanwhile, energy spectrum is trivial under the full periodic boundary condition for the extrinsic higher-order topology. When one direction is open, the system shows the nontrivial topology at each of the edges. Therefore, the intrinsic and the extrinsic second-order topological skin modes are differently localized at the corners. Furthermore, because point gap topology reflects higher-order topology of extended Hermitian Hamiltonians, the results will be generalized to various skin effects due to higher-order topology characterized by different symmetries.

We thank S. Hayashi and K. Osumi for fruitful discussions. This work was supported by JSPS Grant-in-Aid for Scientific Research on Innovative Areas "Discrete Geometric Analysis for Materials Design": Grant No. JP17H06469, and JSPS KAKENHI (Grant No. JP18J22113 and No. JP18J23289).

-
- [1] C. L. Kane and E. J. Mele, Phys. Rev. Lett. **95**, 146802 (2005).
 - [2] C. L. Kane and E. J. Mele, Phys. Rev. Lett. **95**, 226801 (2005).
 - [3] L. Fu and C. L. Kane, Phys. Rev. B **74**, 195312 (2006).
 - [4] L. Fu and C. L. Kane, Phys. Rev. B **76**, 045302 (2007).
 - [5] M. Z. Hasan and C. L. Kane, Rev. Mod. Phys. **82**, 3045 (2010).
 - [6] X.-L. Qi and S.-C. Zhang, Rev. Mod. Phys. **83**, 1057 (2011).
 - [7] Y. Ando and L. Fu, Annual Review of Condensed Matter Physics **6**, 361 (2015).
 - [8] C.-K. Chiu, J. C. Y. Teo, A. P. Schnyder, and S. Ryu, Rev. Mod. Phys. **88**, 035005 (2016).
 - [9] W. A. Benalcazar, B. A. Bernevig, and T. L. Hughes, Science **357**, 61 (2017).
 - [10] W. A. Benalcazar, B. A. Bernevig, and T. L. Hughes, Phys. Rev. B **96**, 245115 (2017).
 - [11] K. Hashimoto, X. Wu, and T. Kimura, Phys. Rev. B **95**, 165443 (2017).
 - [12] Z. Song, Z. Fang, and C. Fang, Phys. Rev. Lett. **119**, 246402 (2017).

- [13] J. Langbehn, Y. Peng, L. Trifunovic, F. von Oppen, and P. W. Brouwer, *Phys. Rev. Lett.* **119**, 246401 (2017).
- [14] F. Schindler, A. M. Cook, M. G. Vergniory, Z. Wang, S. S. Parkin, B. A. Bernevig, and T. Neupert, *Sci. Adv.* **4**, eaat0346 (2018).
- [15] E. Khalaf, H. C. Po, A. Vishwanath, and H. Watanabe, *Phys. Rev. X* **8**, 031070 (2018).
- [16] E. Khalaf, *Phys. Rev. B* **97**, 205136 (2018).
- [17] J. Ahn, D. Kim, Y. Kim, and B.-J. Yang, *Phys. Rev. Lett.* **121**, 106403 (2018).
- [18] A. Matsugatani and H. Watanabe, *Phys. Rev. B* **98**, 205129 (2018).
- [19] M. Lin and T. L. Hughes, *Phys. Rev. B* **98**, 241103(R) (2018).
- [20] T. Fukui and Y. Hatsugai, *Phys. Rev. B* **98**, 035147 (2018).
- [21] M. Geier, L. Trifunovic, M. Hoskam, and P. W. Brouwer, *Phys. Rev. B* **97**, 205135 (2018).
- [22] L. Trifunovic and P. W. Brouwer, *Phys. Rev. X* **9**, 011012 (2019).
- [23] S. Hayashi, *Commun. Math. Phys.* **364**, 343 (2018).
- [24] S. Hayashi, *Lett. Math. Phys.* **109**, 2223 (2019).
- [25] R. Okugawa, S. Hayashi, and T. Nakanishi, *Phys. Rev. B* **100**, 235302 (2019).
- [26] J. Ahn, S. Park, and B.-J. Yang, *Phys. Rev. X* **9**, 021013 (2019).
- [27] Z. Wang, B. J. Wieder, J. Li, B. Yan, and B. A. Bernevig, *Phys. Rev. Lett.* **123**, 186401 (2019).
- [28] M. J. Park, Y. Kim, G. Y. Cho, and S. B. Lee, *Phys. Rev. Lett.* **123**, 216803 (2019).
- [29] E. Lee, R. Kim, J. Ahn, and B.-J. Yang, *npj Quantum Materials* **5**, 1 (2020).
- [30] Y. Tanaka, R. Takahashi, and S. Murakami, *Phys. Rev. B* **101**, 115120 (2020).
- [31] R. Takahashi, Y. Tanaka, and S. Murakami, *Phys. Rev. Research* **2**, 013300 (2020).
- [32] T. Liu, Y.-R. Zhang, Q. Ai, Z. Gong, K. Kawabata, M. Ueda, and F. Nori, *Phys. Rev. Lett.* **122**, 076801 (2019).
- [33] C. H. Lee, L. Li, and J. Gong, *Phys. Rev. Lett.* **123**, 016805 (2019).
- [34] Z. Zhang, M. Rosendo López, Y. Cheng, X. Liu, and J. Christensen, *Phys. Rev. Lett.* **122**, 195501 (2019).
- [35] X.-W. Luo and C. Zhang, *Phys. Rev. Lett.* **123**, 073601 (2019).
- [36] M. Ezawa, *Phys. Rev. B* **99**, 201411(R) (2019).
- [37] V. M. Martinez Alvarez, J. E. Barrios Vargas, M. Berdakin, and L. E. F. Foa Torres, *Eur. Phys. J. special Topics* **227** (2018).
- [38] A. Ghatak and T. Das, *Journal of Physics: Condensed Matter* **31**, 263001 (2019).
- [39] A. Szameit, M. C. Rechtsman, O. Bahat-Treidel, and M. Segev, *Phys. Rev. A* **84**, 021806(R) (2011).
- [40] H. Ramezani, T. Kottos, V. Kovanis, and D. N. Christodoulides, *Phys. Rev. A* **85**, 013818 (2012).
- [41] B. Zhen, C. W. Hsu, Y. Igarashi, L. Lu, I. Kaminer, A. Pick, S.-L. Chua, J. D. Joannopoulos, and M. Soljačić, *Nature* **525**, 354 (2015).
- [42] A. Cerjan, A. Raman, and S. Fan, *Phys. Rev. Lett.* **116**, 203902 (2016).
- [43] Y. Xu, S.-T. Wang, and L.-M. Duan, *Phys. Rev. Lett.* **118**, 045701 (2017).
- [44] H. Shen, B. Zhen, and L. Fu, *Phys. Rev. Lett.* **120**, 146402 (2018).
- [45] V. Kozii and L. Fu, arXiv preprint arXiv:1708.05841 (2017).
- [46] A. Cerjan, M. Xiao, L. Yuan, and S. Fan, *Phys. Rev. B* **97**, 075128 (2018).
- [47] T. Yoshida, R. Peters, and N. Kawakami, *Phys. Rev. B* **98**, 035141 (2018).
- [48] A. A. Zyuzin and A. Y. Zyuzin, *Phys. Rev. B* **97**, 041203(R) (2018).
- [49] J. Carlström and E. J. Bergholtz, *Phys. Rev. A* **98**, 042114 (2018).
- [50] R. Okugawa and T. Yokoyama, *Phys. Rev. B* **99**, 041202(R) (2019).
- [51] J. C. Budich, J. Carlström, F. K. Kunst, and E. J. Bergholtz, *Phys. Rev. B* **99**, 041406(R) (2019).
- [52] W. B. Rui, Y. X. Zhao, and A. P. Schnyder, *Phys. Rev. B* **99**, 241110(R) (2019).
- [53] H. Zhou, J. Y. Lee, S. Liu, and B. Zhen, *Optica* **6**, 190 (2019).
- [54] T. Yoshida, R. Peters, N. Kawakami, and Y. Hatsugai, *Phys. Rev. B* **99**, 121101(R) (2019).
- [55] Z. Yang and J. Hu, *Phys. Rev. B* **99**, 081102(R) (2019).
- [56] H. Wang, J. Ruan, and H. Zhang, *Phys. Rev. B* **99**, 075130 (2019).
- [57] K. Moors, A. A. Zyuzin, A. Y. Zyuzin, R. P. Tiwari, and T. L. Schmidt, *Phys. Rev. B* **99**, 041116(R) (2019).
- [58] A. A. Zyuzin and P. Simon, *Phys. Rev. B* **99**, 165145 (2019).
- [59] X. Zhang, K. Ding, X. Zhou, J. Xu, and D. Jin, *Phys. Rev. Lett.* **123**, 237202 (2019).
- [60] A. Cerjan, S. Huang, M. Wang, K. P. Chen, Y. Chong, and M. C. Rechtsman, *Nat. Photonics* **13**, 623 (2019).
- [61] J. Carlström, M. Stålhammar, J. C. Budich, and E. J. Bergholtz, *Phys. Rev. B* **99**, 161115(R) (2019).
- [62] T. Yoshida and Y. Hatsugai, *Phys. Rev. B* **100**, 054109 (2019).
- [63] K. Kawabata, T. Bessho, and M. Sato, *Phys. Rev. Lett.* **123**, 066405 (2019).
- [64] K. Kimura, T. Yoshida, and N. Kawakami, *Phys. Rev. B* **100**, 115124 (2019).
- [65] K. Yokomizo and S. Murakami, arXiv preprint arXiv:2001.07348 (2020).
- [66] Z. Gong, Y. Ashida, K. Kawabata, K. Takasan, S. Higashikawa, and M. Ueda, *Phys. Rev. X* **8**, 031079 (2018).
- [67] S. Yao and Z. Wang, *Phys. Rev. Lett.* **121**, 086803 (2018).
- [68] S. Yao, F. Song, and Z. Wang, *Phys. Rev. Lett.* **121**, 136802 (2018).
- [69] F. K. Kunst, E. Edvardsson, J. C. Budich, and E. J. Bergholtz, *Phys. Rev. Lett.* **121**, 026808 (2018).
- [70] C. H. Lee and R. Thomale, *Phys. Rev. B* **99**, 201103(R) (2019).
- [71] M. Ezawa, *Phys. Rev. B* **99**, 121411(R) (2019).
- [72] K. Yokomizo and S. Murakami, *Phys. Rev. Lett.* **123**, 066404 (2019).
- [73] F. Song, S. Yao, and Z. Wang, *Phys. Rev. Lett.* **123**, 170401 (2019).
- [74] F. Song, S. Yao, and Z. Wang, *Phys. Rev. Lett.* **123**, 246801 (2019).
- [75] S. Longhi, *Phys. Rev. Research* **1**, 023013 (2019).
- [76] N. Okuma and M. Sato, *Phys. Rev. Lett.* **123**, 097701 (2019).
- [77] N. Okuma, K. Kawabata, K. Shiozaki, and M. Sato, *Phys. Rev. Lett.* **124**, 086801 (2020).

- [78] D. S. Borgnia, A. J. Kruchkov, and R.-J. Slager, *Phys. Rev. Lett.* **124**, 056802 (2020).
- [79] K. Kawabata, N. Okuma, and M. Sato, *Phys. Rev. B* **101**, 195147 (2020).
- [80] T. Hofmann, T. Helbig, F. Schindler, N. Salgo, M. Brzezińska, M. Greiter, T. Kiessling, D. Wolf, A. Vollhardt, A. Kabaši, C. H. Lee, A. Bilušić, R. Thomale, and T. Neupert, *Phys. Rev. Research* **2**, 023265 (2020).
- [81] K. Zhang, Z. Yang, and C. Fang, arXiv:1910.01131.
- [82] Z. Yang, K. Zhang, C. Fang, and J. Hu, arXiv:1912.05499.
- [83] T. Yoshida, T. Mizoguchi, and Y. Hatsugai, *Phys. Rev. Research* **2**, 022062 (2020).
- [84] Y. Yi and Z. Yang, arXiv:2003.02219.
- [85] C.-H. Liu, K. Zhang, Z. Yang, and S. Chen, arXiv:2005.02617.
- [86] T. Helbig, T. Hofmann, S. Imhof, M. Abdelghany, T. Kiessling, L. Molenkamp, C. Lee, A. Szameit, M. Greiter, and R. Thomale, *Nat. Phys.* **16**, 747 (2020).
- [87] L. Xiao, T. Deng, K. Wang, G. Zhu, Z. Wang, W. Yi, and P. Xue, *Nat. Phys.* **16**, 761 (2020).
- [88] A. McDonald, T. Pereg-Barnea, and A. A. Clerk, *Phys. Rev. X* **8**, 041031 (2018).
- [89] S. Longhi, *Phys. Rev. Lett.* **124**, 066602 (2020).
- [90] T. Yu, Y.-X. Zhang, S. Sharma, X. Zhang, Y. M. Blanter, and G. E. W. Bauer, *Phys. Rev. Lett.* **124**, 107202 (2020).
- [91] L. Li, C. H. Lee, and J. Gong, *Phys. Rev. Lett.* **124**, 250402 (2020).
- [92] H. Zhou and J. Y. Lee, *Phys. Rev. B* **99**, 235112 (2019).
- [93] C.-H. Liu, H. Jiang, and S. Chen, *Phys. Rev. B* **99**, 125103 (2019).
- [94] K. Kawabata, K. Shiozaki, M. Ueda, and M. Sato, *Phys. Rev. X* **9**, 041015 (2019).
- [95] S. Ono and H. Watanabe, *Phys. Rev. B* **98**, 115150 (2018).
- [96] See Supplemental Material, which includes Refs. [97–100].
- [97] I. Mondragon-Shem, T. L. Hughes, J. Song, and E. Prodan, *Phys. Rev. Lett.* **113**, 046802 (2014).
- [98] T. L. Hughes, E. Prodan, and B. A. Bernevig, *Phys. Rev. B* **83**, 245132 (2011).
- [99] A. M. Turner, Y. Zhang, R. S. K. Mong, and A. Vishwanath, *Phys. Rev. B* **85**, 165120 (2012).
- [100] J. C. Y. Teo, L. Fu, and C. L. Kane, *Phys. Rev. B* **78**, 045426 (2008).

Supplemental material for "Second-order topological non-Hermitian skin effects"

Ryo Okugawa,¹ Ryo Takahashi,² and Kazuki Yokomizo²

¹*Graduate School of Information Sciences, Tohoku University, Sendai 980-8579, Japan*

²*Department of Physics, Tokyo Institute of Technology,
2-12-1 Ookayama, Meguro-ku, Tokyo, 152-8551, Japan*

I. INTRINSIC SECOND-ORDER TOPOLOGY PROTECTED BY INVERSION SYMMETRY

A. The relationship between the bulk parity invariant and the winding number for ribbon geometry

To obtain skin modes localized only at corners in 2D systems, we need to calculate the winding number under the system which is open in one direction. In this section, we reveal a relationship between the winding number and the bulk parity invariant μ_j for the extended Hermitian Hamiltonian with inversion symmetry. When the x_j direction is open, we show that the winding number is given by

$$W_{x_j-OBC} = \frac{\mu_j}{2} \pmod{2}. \quad (S1)$$

Therefore, if $\mu_j = 2$, the correspondent non-Hermitian Hamiltonian shows skin modes localized at the corner.

We begin with the winding number for 1D chiral-symmetric Hermitian systems in the presence of inversion symmetry. The winding number can be expressed by the number of negative parity eigenvalues below zero energy at $k = 0$ and π . The winding number is rewritten as [1–4]

$$(-1)^W = (-1)^{n_-(0) - n_-(\pi)}, \quad (S2)$$

where $n_-(0)$ and $n_-(\pi)$ are the number of negative parity eigenvalues below zero energy at $k = 0$ and π , respectively. In 2D systems with inversion and chiral symmetries, the ribbon geometry with the x_j direction open can be regarded as 1D. Thus, we can obtain the winding number W_{x_j-OBC} by applying Eq. (S2) to the ribbon geometry.

Under the OBC in the x_j direction in the 2D system, we denote the number of the negative parity eigenvalues below zero energy at $k = 0$ (π) as $\tilde{n}_-^{x_j}(0)$ ($\tilde{n}_-^{x_j}(\pi)$). Here, we assume that the bands are gapped at zero energy both under the PBC and under the OBC in the x_j direction. Then, the band structures do not have the nontrivial first-order topology on the assumption. According to Ref. 5, the parity invariants $\tilde{n}_-^{x_j}(0)$ and $\tilde{n}_-^{x_j}(\pi)$ can be obtained via cutting procedure which relates the PBC to the OBC [6]. From the procedure, $\tilde{n}_-^{x_j}(0)$ and $\tilde{n}_-^{x_j}(\pi)$ are related to the number of the 2D negative parity eigenvalues under the PBC. The relationships are [5]

$$\tilde{n}_-^x(0) = \frac{N_{OBC}^x(0) - n_{PBC}}{2} + \frac{n_-(0,0) + n_-(\pi,0)}{2}, \quad (S3)$$

$$\tilde{n}_-^x(\pi) = \frac{N_{OBC}^x(\pi) - n_{PBC}}{2} + \frac{n_-(0,\pi) + n_-(\pi,\pi)}{2}, \quad (S4)$$

$$\tilde{n}_-^y(0) = \frac{N_{OBC}^y(0) - n_{PBC}}{2} + \frac{n_-(0,0) + n_-(0,\pi)}{2}, \quad (S5)$$

$$\tilde{n}_-^y(\pi) = \frac{N_{OBC}^y(\pi) - n_{PBC}}{2} + \frac{n_-(\pi,0) + n_-(\pi,\pi)}{2}, \quad (S6)$$

where $N_{OBC}^{x_j}(0)$ and $N_{OBC}^{x_j}(\pi)$ are the number of occupied states under the OBC in the x_j direction, and n_{PBC} is the number of occupied bands under the PBC. We have $N_{OBC}^{x_j}(0) = N_{OBC}^{x_j}(\pi)$ since the bands are assumed to be gapped at zero energy under the OBC. Therefore, we obtain

$$\tilde{n}_-^{x_j}(0) - \tilde{n}_-^{x_j}(\pi) = \frac{\mu_j}{2}. \quad (S7)$$

As a result, Eq. (S1) is proved by Eqs. (S2) and (S7). Because the winding number for corner modes can be determined by the bulk parity invariant, the second-order topology is intrinsic.

Figure S1 illustrates examples for $\mu_x = \mu_y = 2$. The extended Hermitian Hamiltonian can have $\mu_i = 2$ when double band inversion occurs at an odd number of the inversion-invariant momenta. Inversion symmetry needs to anticommute with chiral symmetry to change μ_i through double band inversion [7].

Henceforth, we consider how to realize systems with $\mu_j = 2$. To do so, we use a non-Hermitian Hamiltonian H which gives time-reversal symmetry \tilde{T} with $\tilde{T}^2 = -1$ to the extended Hermitian Hamiltonian \tilde{H} . In this case, we can compute the \mathbb{Z}_2 Kane-Mele topological invariant under the PBC [8–10]. If H also gives inversion symmetry \tilde{I} to \tilde{H} from Eq. (6), the \mathbb{Z}_2 invariant can be calculated from the number of negative parity eigenvalues at time-reversal invariant momenta (TRIM) below zero energy [10]. Because of Kramers degeneracy, the \mathbb{Z}_2 invariant is given by

$$(-1)^\nu = (-1)^{\sum_i n_-(\Gamma_i)/2}. \quad (S8)$$

The sum is taken over all the TRIM in the 2D bulk momentum space. Therefore, when \tilde{H} shows bulk parity eigenvalues in Figs. S1 (a) and (b), the \mathbb{Z}_2 topology is nontrivial. Then, if we slightly break only the time-reversal symmetry in the \mathbb{Z}_2 nontrivial case, we realize double band inversion for $\mu_j = 2$ as long as the band gap is open.

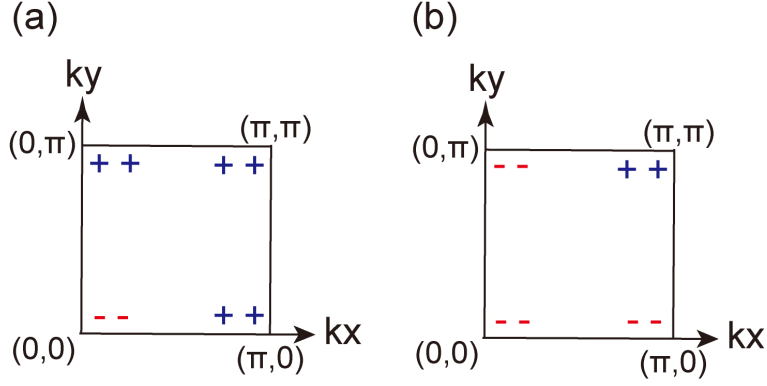


FIG. S1. Illustrative examples of parity eigenvalues below zero energy to give $\mu = 2$. The signs $+$ ($-$) indicate the parity eigenvalues below zero energy at the inversion-invariant momenta. In these cases, the system is not first-order topological. When $m - 2c - |\mathbf{B}| < E < m - |\mathbf{B}|$ and $m + |\mathbf{B}| < E < m + 2c - |\mathbf{B}|$, the model $\tilde{H}_{int}(\mathbf{k})$ realizes (a) and (b), respectively.

B. Calculation of the nontrivial parity invariant μ for the skin modes in the model

By using the discussion in Sec. I A, we show how to obtain $\mu_{i=x,y}(E) = 2$ for \tilde{H}_{int} in Eq. (5) in the main text. The nontrivial parity invariants yield the intrinsic second-order topological skin effect for H_{int} in Eq. (4) in the main text. We here calculate parity eigenvalues for the extended Hermitian Hamiltonian with the real reference energy.

To realize $\mu_j = 2$, we ignore the parameter \mathbf{B} at first. When $\mathbf{B} = 0$ and E is real, the extended Hermitian Hamiltonian in Eq. (5) has not only inversion symmetry but also time-reversal symmetry. The time-reversal symmetry is represented by $\tilde{T} = -i\sigma_1 \otimes \sigma_2 K$, where K is complex conjugation. Therefore, Kramers degeneracy arises because $\tilde{T}^2 = -1$. At all the TRIM Γ_i , we can analytically obtain parity eigenvalues $\xi(\Gamma_i)$ for the Kramers pair below zero energy. By putting $h(\mathbf{k}) = -(m - E - c \sum_{j=x,y} \cos k_j)$, the parity eigenvalues are

$$\xi(\Gamma_i) = -\text{sgn}(h(\Gamma_i)). \quad (\text{S9})$$

In this model, $n_-(\Gamma_i) = 2(0)$ if $\xi(\Gamma_i)$ is negative (positive) since Kramers degeneracy is present. For the time-reversal symmetric model, we can easily obtain the \mathbb{Z}_2 Kane-Mele topological invariant ν . From Eqs. (S8) and (S9), the topological invariant ν is obtained from

$$(-1)^{\nu(E)} = \text{sgn}(m - E - 2c) \text{sgn}(m - E + 2c). \quad (\text{S10})$$

Because m and c are positive in the model, $\nu(E) = 1$, i.e. $\mu(E) = 2$ when $m - 2c < E < m + 2c$ except $E = m$. $h(0, \pi) = h(\pi, 0)$ leads to $n_-(0, \pi) = n_-(\pi, 0)$, and therefore we have $\mu_x = \mu_y = \mu$. If an odd number of the TRIM gives the negative parity eigenvalues, this model has $\nu = 1$, and then $\mu = 2$.

We need to add the parameters $\mathbf{B} = (B_x, B_y)$ to $\tilde{H}_{int}(\mathbf{k})$ in order to break the time-reversal symmetry. Then, the invariant $\mu = 2$ detects the winding number for inversion-symmetric 1D ribbon geometry. As long as the bulk gap keeps open, the value of μ is preserved even though \mathbf{B} is added. As a result, we can obtain $\mu = 2$ in the absence of the time-reversal symmetry if the finite \mathbf{B} does not close the bulk gap.

For the extended Hermitian Hamiltonian $\tilde{H}_{int}(\mathbf{k})$, the energy eigenvalues at Γ_i are $\pm|h(\Gamma_i)| \pm |\mathbf{B}|$. Therefore, when a reference energy E satisfies $|h(\Gamma_i)| = |\mathbf{B}|$, $\mu(E)$ changes at the energy. Hence, if $|\mathbf{B}|$ is sufficiently small, we obtain $\mu(E) = 2$ for the real E in the region $m - 2c - |\mathbf{B}| < E < m - |\mathbf{B}|$ or $m + |\mathbf{B}| < E < m + 2c - |\mathbf{B}|$. In the ribbon geometry, the system realizes the nonzero winding number near the regions which give second-order topological skin modes [Fig. 1 (c)]. On the other hand, when $E < m - 2c - |\mathbf{B}|$ or $E > m + 2c - |\mathbf{B}|$, the topology is trivial in terms of both the first order and the second-order topology. The other regions of the real energy axis give the nontrivial first-order topology. Therefore, we can find skin modes around the first-order topological regions under the OBC in one direction, as seen in Fig. 1 (b) in the main text.

II. EXTRINSIC SECOND-ORDER TOPOLOGY WITH ONLY CHIRAL SYMMETRY

A. Edge gap-closing and change of the topological invariant ν_{2D}

We discuss how gap closing on edges changes the extrinsic second-order topology for $\tilde{H}'_{ext}(\mathbf{k})$ in Eq. (7) in the main text. The topological invariant $\nu_{2D} = w_x w_y$ is defined for the matrix form in Eq. (7). The extrinsic second-order topology leads to edge bands with nontrivial winding structures. In this section, we explain that change of ν_{2D} accompanies the edge gap-closing, according to Ref. [11–13].

Suppose that a phase transition happens from a trivial phase with $(w_x, w_y) = (0, -1)$ to a topological phase with $(-1, -1)$. In this case, the band gap closes at zero energy on the edges periodic in the x direction. To see this, we consider the semi-infinite system with one edge periodic in the x direction. In other words, we impose the OBC in the y direction on the system. Since \mathcal{H}_y is nontrivial thanks to $w_y = -1$, there is a zero mode ϕ_y^{zero} which satisfies $\mathcal{H}_y^{OBC} \phi_y^{zero} = 0$. Thus, \tilde{H}'_{ext} under the semi-infinite OBC has edge states represented by $\psi_n(k_x) \otimes \phi_y^{zero}$, where $\psi_n(k_x)$ is the Bloch wavefunction for $\mathcal{H}_x(k_x)$. Because w_x changes the value from 0 to -1 , any of the Bloch wavefunctions need to take the zero-valued eigenvalues. As a result, the edge states $\psi_n(k_x) \otimes \phi_y^{zero}$ closes the gap at zero energy. In a similar way, if the system enters a topological phase with $(-1, -1)$ from a trivial phase with $(-1, 0)$, gap closing occurs on the edges periodic in the y direction. Eventually, the edge states close the gap at zero energy when ν_{2D} changes, which gives the nonzero winding number W for the edge bands [14], as shown in Fig. 2(c) in the main text.

Additionally, we can easily find the topological corner zero-energy modes in this model \tilde{H}'_{ext} as follows. We assume that both $\mathcal{H}_x(k_x)$ and $\mathcal{H}_y(k_y)$ are topologically nontrivial, i.e., $\nu_{2D} \neq 0$. Let us denote a zero mode as ϕ_i^{zero} for \mathcal{H}_i under semi-infinite OBCs. Then, the system shows a topological corner mode given by $\phi_x^{zero} \otimes \phi_y^{zero}$ under the semi-infinite OBC with one corner. From this discussion, we can also see that the edges are nontrivial.

B. Calculation of the extrinsic second-order topology for the skin modes in the model

The model $H_{ext}(\mathbf{k})$ in Eq. (9) in the main text shows skin modes localized at the corners. To clarify the origin, we study extrinsic second-order topology of the extended Hermitian Hamiltonian. Here, we show that the system has reference points with the nonzero ν_{2D} for the nonzero winding numbers on the edges, which realizes the extrinsic second-order topological skin effect.

When the reference energy is real, we can easily show that the extended Hermitian Hamiltonian of $H_{ext}(\mathbf{k})$ can have the extrinsic second-order topology. The extended Hermitian Hamiltonian under the PBC is given by

$$\tilde{H}_{ext}(\mathbf{k}) = \begin{pmatrix} 0 & H_{ext}(\mathbf{k}) - E \\ H_{ext}^\dagger(\mathbf{k}) - E & 0 \end{pmatrix} \quad (\text{S11})$$

In order to investigate the second-order topology, we perform unitary transformation for $H_{ext}(\mathbf{k})$ represented as

$$U = \begin{pmatrix} 0 & 0 & 0 & -1 \\ 1 & 0 & 0 & 0 \\ 0 & -1 & 0 & 0 \\ 0 & 0 & 1 & 0 \end{pmatrix}. \quad (\text{S12})$$

Then, we obtain the following Hamiltonian:

$$\begin{aligned} \tilde{H}'_{ext}(\mathbf{k}) &= U \tilde{H}_{ext}(\mathbf{k}) U^\dagger \\ &= \mathcal{H}_x(k_x) \otimes \tau_0 + \tau_z \otimes \mathcal{H}_y(k_y). \end{aligned} \quad (\text{S13})$$

Here, $\mathcal{H}'_{x,y}(k_{x,y})$ in Eq. (S13) are

$$\mathcal{H}_x(k_x) = (2t_x \cos k_x - E)\tau_x + 2g_x \sin k_x \tau_y, \quad (\text{S14})$$

$$\mathcal{H}_y(k_y) = 2t_y \cos k_y \tau_x + 2g_y \sin k_y \tau_y. \quad (\text{S15})$$

Because \mathcal{H}_x and \mathcal{H}_y have chiral symmetry τ_z , $\tilde{H}'_{ext}(\mathbf{k})$ can be included in the Hamiltonians given by Eq. (7). The winding number for \mathcal{H}_y are $w_y = -\text{sgn}(g_y)$ since t_y is positive now. On the other hand, the winding number w_x for \mathcal{H}_x depends on the reference energy E . Thus, while $w_x(E) = -\text{sgn}(g_x)$ when $-2t_x < E < 2t_x$, the value becomes zero in the other regions on the real energy axis. Hence, we obtain the nonzero $\nu_{2D}(E) = \text{sgn}(g_x)\text{sgn}(g_y)$ if and only if $-2t_x < E < 2t_x$.

As discussed in Sec. II A, the Hermitian model in Eq. (S13) shows topological phase transitions on the edges when the topological invariant ν_{2D} changes. The correspondent non-Hermitian Hamiltonian also closes point gap at the reference energy E . Indeed, if (w_x, w_y) changes from $(0, -1)$ to $(-1, -1)$, the gap closing needs to happen on edges along the y direction [11–13]. Therefore, the point gap closes at $E = \pm 2t_x$ on the edges periodic in the y direction, as seen in Fig. 2(c). Consequently, the winding number can be finite on the edges.

-
- [1] I. Mondragon-Shem, T. L. Hughes, J. Song, and E. Prodan, Phys. Rev. Lett. **113**, 046802 (2014).
 - [2] T. L. Hughes, E. Prodan, and B. A. Bernevig, Phys. Rev. B **83**, 245132 (2011).
 - [3] A. M. Turner, Y. Zhang, R. S. K. Mong, and A. Vishwanath, Phys. Rev. B **85**, 165120 (2012).
 - [4] W. A. Benalcazar, B. A. Bernevig, and T. L. Hughes, Phys. Rev. B **96**, 245115 (2017).
 - [5] R. Takahashi, Y. Tanaka, and S. Murakami, Phys. Rev. Research **2**, 013300 (2020).
 - [6] J. C. Y. Teo, L. Fu, and C. L. Kane, Phys. Rev. B **78**, 045426 (2008).
 - [7] E. Khalaf, Phys. Rev. B **97**, 205136 (2018).
 - [8] C. L. Kane and E. J. Mele, Phys. Rev. Lett. **95**, 146802 (2005).
 - [9] L. Fu and C. L. Kane, Phys. Rev. B **74**, 195312 (2006).
 - [10] L. Fu and C. L. Kane, Phys. Rev. B **76**, 045302 (2007).
 - [11] S. Hayashi, Commun. Math. Phys. **364**, 343 (2018).
 - [12] S. Hayashi, Lett. Math. Phys. **109**, 2223 (2019).
 - [13] R. Okugawa, S. Hayashi, and T. Nakanishi, Phys. Rev. B **100**, 235302 (2019).
 - [14] We do not consider a phase transition from a trivial phase with $(w_x, w_y) = (0, 0)$ to a topological phase with $(-1, -1)$ because the phase transtion happens from the bulk gap closing.